Inorganic Chemistry

pubs.acs.org/IC

Article

Rhenium Alkyne Catalysis: Sterics Control the Reactivity

Michele Tomasini, Martí Gimferrer,* Lucia Caporaso,* and Albert Poater*

Cite This: *Inorg. Chem.* 2024, 63, 5842−5851

Read Online

ACCESS | Metrics & More | Article Recommendations | Supporting Information

ABSTRACT: Metathesis reactions, including alkane, alkene, and alkyne metatheses, have their origins in the fundamental understanding of chemical reactions and the development of specialized catalysts. These reactions stand as transformative pillars in organic chemistry, providing efficient rearrangement of carbon−carbon bonds and enabling synthetic access to diverse and complex compounds. Their impact spans industries such as petrochemicals, pharmaceuticals, and materials science. In this work, we present a detailed mechanistic study of the Re(V) catalyzed alkyne metathesis through density functional theory calculations. Our findings are in agreement with the experimental evidence from Jia and co-workers and unveil critical factors governing catalyst performance. Our work not only enhances our understanding of alkyne metathesis but also contributes to the broader landscape of catalytic processes, facilitating the design of more efficient and selective transformations in organic synthesis.

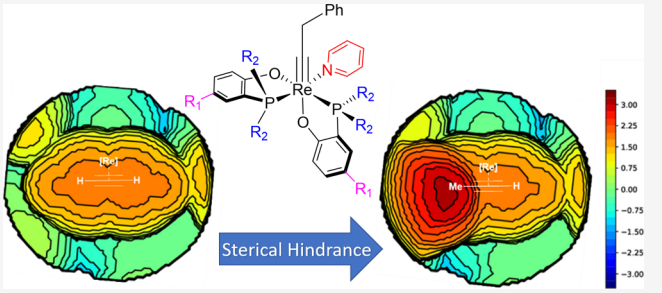

INTRODUCTION

Metathesis reactions are pivotal transformations involving the reshuffling of carbon−carbon (C−C) bonds of different multiplicities—namely, single, double, and triple C−C bonds for alkane, alkene, and alkyne metathesis, respectively. Alkane metathesis, for instance, entails the redistribution of single C−C bonds within alkanes, yielding a different alkane product. This transformation traces its roots to pioneering work in novel catalyst design capable of selectively breaking and reassembling alkane C−C bonds, paving the way for subsequent advancements.[1,2] These seminal studies not only unveiled the potential of alkane metathesis in converting simple hydrocarbons into more intricate ones but also underscored its applicability across diverse sectors, e.g., the petrochemical industry.

Similarly, alkene metathesis involves the reorganization of C−C double bonds in alkenes, originating in the early 1970s with Chauvin's elucidation of its mechanistic intricacies.[3] Subsequent breakthroughs by Grubbs and Schrock yielded efficient catalysts for this reaction, facilitating its practical application (Scheme 1a).[4,5] Alkyne metathesis, albeit to a lesser extent,[6,7] emerged as a versatile strategy for synthesizing complex molecules, finding utility in various organic chemistry procedures,[8,9] including ring-opening alkyne polymerization,[10] and the synthesis of conjugated polymers via metathesis of acyclic diynes.[11,12]

In the 1980s, Schrock and co-workers developed the first homogeneous catalysts for alkyne metathesis (Scheme 1b),[13] based on well-defined d^0 W(VI) and Mo(VI) alkylidyne catalysts. This marked a departure from earlier heterogeneous catalysts consisting of WO_3/silica, which operated only under high temperatures exceeding 200 °C.[14] Subsequent homogeneous catalysts were reported, involving a mixture of $Mo(CO)_6$ and phenols, capable of functioning in high-boiling-point solvents (around 150 °C).[15] Due to their activity and stability, Mo-based catalysts garnered increasing interest, resulting in the development of highly efficient d^0 W(VI)/Mo(VI) alkylidyne

Scheme 1. Reference Catalysts for Alkene Metathesis (a), and Example Catalysts for Alkyne Metathesis (b)

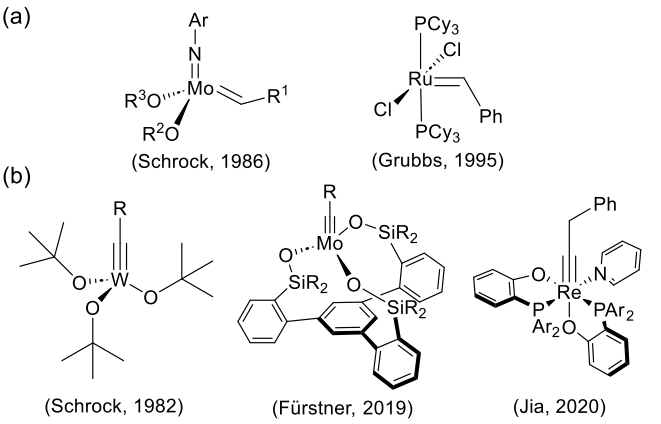

Received: November 28, 2023
Revised: February 27, 2024
Accepted: March 5, 2024
Published: March 20, 2024

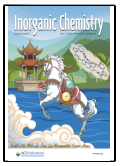

https://doi.org/10.1021/acs.inorgchem.3c04235
Inorg. Chem. 2024, 63, 5842−5851

catalysts with customizable ligand systems, encompassing fluorinated alkoxides,[16] silanolates,[17] and unconventional combinations of electron-withdrawing alkoxides with imido,[18] amido,[19] silanolate,[20] and NHC ligands.[21]

Chronologically, Mo(VI) alkylidyne precursors with monodentate[22] or polydentate[23] alcohol preceded the development of Mo(VI)/W(VI) canopy catalysts with a tridentate silanolate ligand, pioneered by the Fürstner[24] and Lee research groups.[25] These catalysts exhibited remarkable compatibility with protic functional groups, even in the presence of traces of water. Subsequently, the Zhang group reported in situ-formed catalytic systems capable of performing alkyne metathesis under open-air conditions.[26]

Beyond the traditional d^0 Mo/W systems, Schrock[27] proposed non-d^0 transition-metal (TM) alkylidyne complexes,[28] enhancing the catalysts stability and substrate scope. Note that examples of this type of systems increased substantially in the last years.[29] Since the insights reported by Ehrhorn and Tamm,[7] this challenge remained unexplored until 2020 with the disclosure of a d^2 Re(V) alkylidyne by Williams, Jia, and co-workers. This complex exhibited low activity yet remarkable air stability, catalyzing alkyne metathesis in the presence of traces of water and demonstrating compatibility with a wide range of functional groups (see Scheme 2a).[30]

Scheme 2. d^2 Re(V) Alkylidyne Complexes for Catalytic Alkyne Metathesis Synthesized in (a) 2020 and (b) 2022 by Williams, Jia, and Co-Workers[30,31]

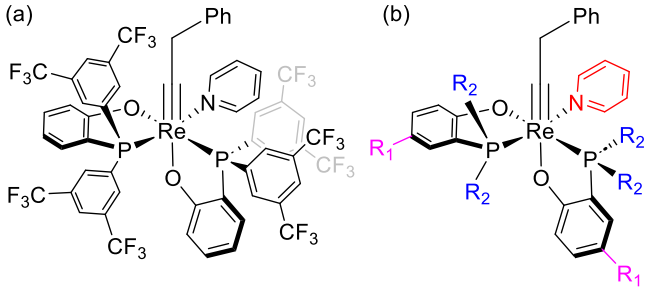

Subsequent work by the same team unveiled a series of Re(V) alkylidyne complexes featuring phosphino-phenolate (PO) bidentate ligands,[31] each possessing distinct electronic and steric properties.[32] Significantly, this research achieved a noteworthy milestone by showcasing, for the first time, the catalysis of non-d^0 alkylidyne complexes in ring-closing alkyne metathesis (RCAM) for the first time. This breakthrough allows establishing a clear dependence between the high activity of these catalysts and their structural characteristics within this family of systems. This correlation sheds light on the factors influencing their performance in alkyne metathesis reactions. However, a complete understanding of the mechanism remains elusive, prompting the need for detailed investigations.

Motivate by these advancements, in this work, we unveil the mechanism of alkyne metathesis catalyzed by a formally d^2 Re(V) alkylidyne complex (see Scheme 2b, with R_1 = H and R_2 = Ph) by means of density functional theory (DFT) calculations. Moreover, we investigate the steric and electronic properties of differently substituted PO ligands and their impact on the catalytic activity, aiming to enhance predictive capabilities in Re-based alkyne catalysts design.[33]

COMPUTATIONAL DETAILS

All DFT calculations were performed with the Gaussian16 package.[34] Geometry optimizations were performed using the BP86 functional, a pure GGA functional developed by Becke and Perdew,[35] including the Grimme D3 dispersion correction. These calculations were performed in conjunction with the all electron double-ζ polarized def2-SVP basis set for light atoms,[36] whereas for Re the SDD basis set (and pseudopotential) has been employed.[37] All optimizations were carried out without symmetry constraints, and the nature of the stationary points was confirmed by analytical frequency analysis. Gibbs free energies at 373.15 K were calculated using the electronic energy evaluated with the M06 functional,[38] and the triple-ζ basis set def2-TZVP for all the atoms,[39] except for Re that used again the SDD basis set (and pseudopotential). Furthermore, solvent effects were estimated with the universal solvation model SMD from Cramer and Truhlar using toluene as solvent.[40] The reported Gibbs free energies encompass electronic energies obtained at the M06/def2-TZVP(SMD(toluene))~SDD//BP86-D3/def2-SVP~SDD level of theory. These values were corrected with zero-point vibrational energies, thermal corrections, and entropy effects computed at the BP86-D3/def2-SVP~SDD level.

RESULTS AND DISCUSSION

Let us start with the mechanistic study of the replacement of a pyridine ligand from precatalyst species **R** by an acetylene molecule. For this rather simple process, two possible pathways exist, associative and dissociative, being both considered and evaluated. The results for both pathways, including the relative Gibbs energies of the involved species obtained at the M06/def2-TZVP~SDD(SMD(toluene))//BP86-D3/def2-SVP~SDD level of theory, are gathered in Figure 1. In the associative pathway, the acetylene molecule first approaches the precatalyst species **R**, provoking the Re−N bond breaking and coordinating in a η^2-fashion, forming species **A** (ΔG = 3.5 kcal/mol) through a hepta-coordinated transition state $\mathbf{TS_{R\rightarrow A}}$ ($\Delta G^{\ddagger}$ = 30.4 kcal/mol). This strained transition state suffers the π-conflict paradox, i.e., the repulsion between pπ electrons of the entering alkyne and the M−C triple bond dπ electrons.[41] Alternatively, the dissociation pathway (Figure 1) involves the formation of species **A** in two steps. First, the pyridine ligand is released (to the solvent media) via $\mathbf{TS_{R\rightarrow A0}}$ ($\Delta G^{\ddagger}$ = 27.2 kcal/mol), forming the coordinatively unsaturated (vacant site present), unstable and thus highly reactive intermediate **A0** (ΔG = 15.4 kcal/mol). Then, the latter intermediate reacts with acetylene to form **A** through $\mathbf{TS_{A0\rightarrow A}}$ ($\Delta G^{\ddagger}$ = 22.3 kcal/mol). Overall, the associative mechanism, which is coincident with the concerted mechanism as well, through $\mathbf{TS_{R\rightarrow A}}$ is kinetically unfavored (30.4 vs 27.2 kcal/mol) and not plausible under the reported reaction conditions (T = 100 °C), being ruled out. Instead, the octahedral alkyne−alkylidyne complex **A** is formed thanks to the pyridine ligand dissociation and the alkyne can work as a 4e-donor.[42] Once **A** is formed, the reaction, i.e., the activation, can proceed (Figure 2) through a cycloaddition step leading to the rhenacyclobutadiene **B** (ΔG = 7.4 kcal/mol) via $\mathbf{TS_{A\rightarrow B}}$ ($\Delta G^{\ddagger}$ = 20.0 kcal/mol). However, the formation of species **C** from **B** requires an enormous amount of energy ($\Delta G^{\ddagger}_{\mathrm{TSB\rightarrow C}}$ = 44.5 kcal/mol), which is kinetically impossible. **A** is the Δ-*cis* isomer depicted in red in Figure 2, and its isomer **Λ-*cis*A** exists, depicted in

https://doi.org/10.1021/acs.inorgchem.3c04235
Inorg. Chem. 2024, 63, 5842−5851

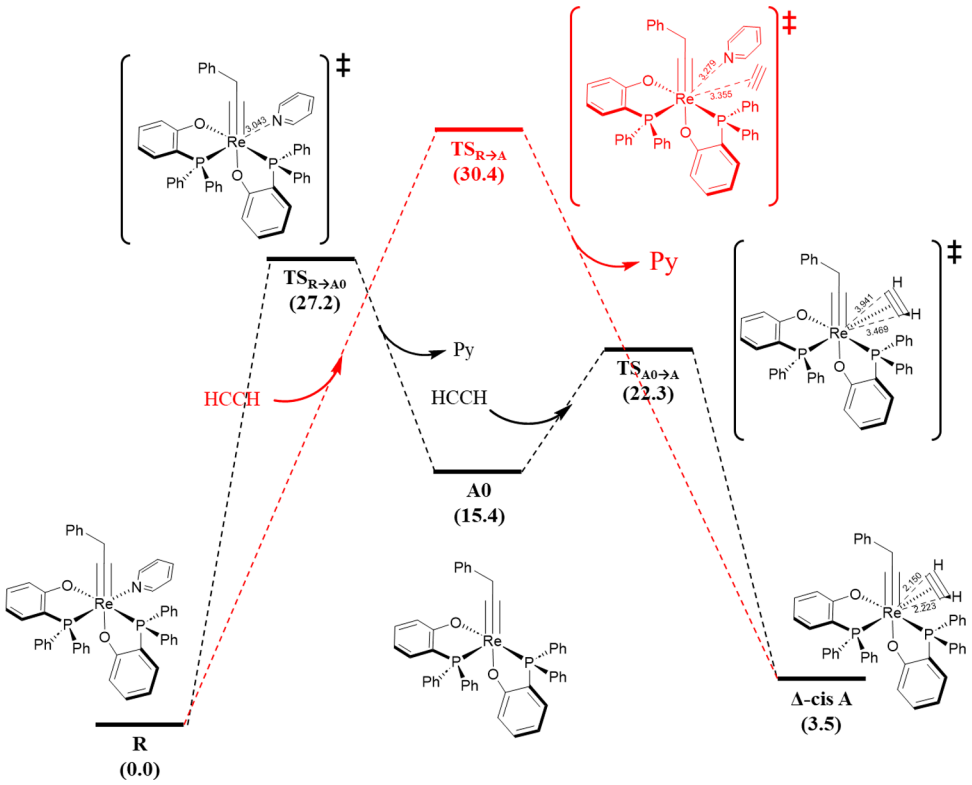

Figure 1. Reaction pathway for exchange of the pyridine (py) by the alkyne substrate on the rhenium complex **R** (relative Gibbs free energies in kcal/mol and selected distances in Å).

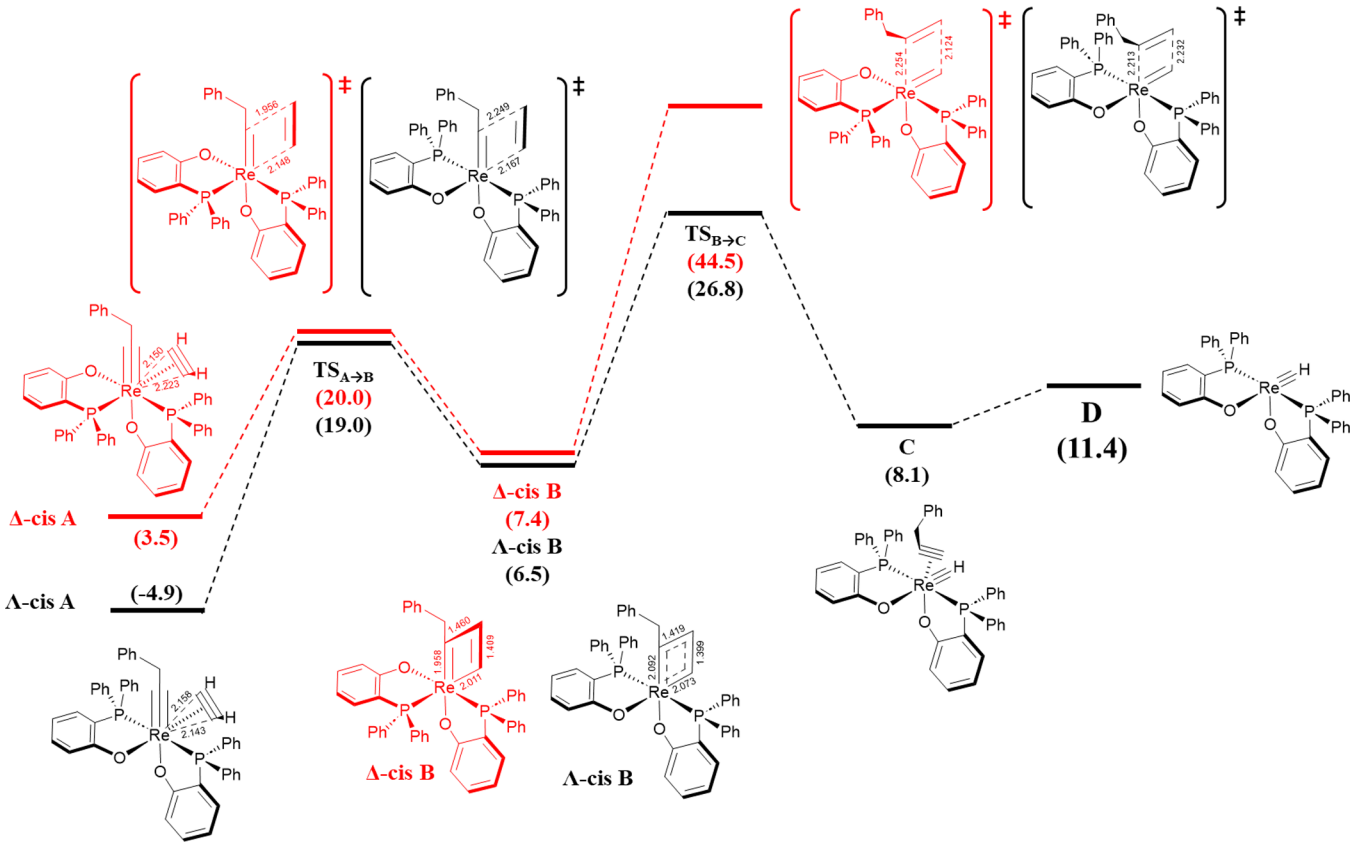

Figure 2. Activation pathway for the formation of the rhenium complex **D**, the catalytic active species for alkyne metathesis (relative Gibbs free energies in kcal/mol and selected distances in Å).

https://doi.org/10.1021/acs.inorgchem.3c04235
Inorg. Chem. 2024, 63, 5842−5851

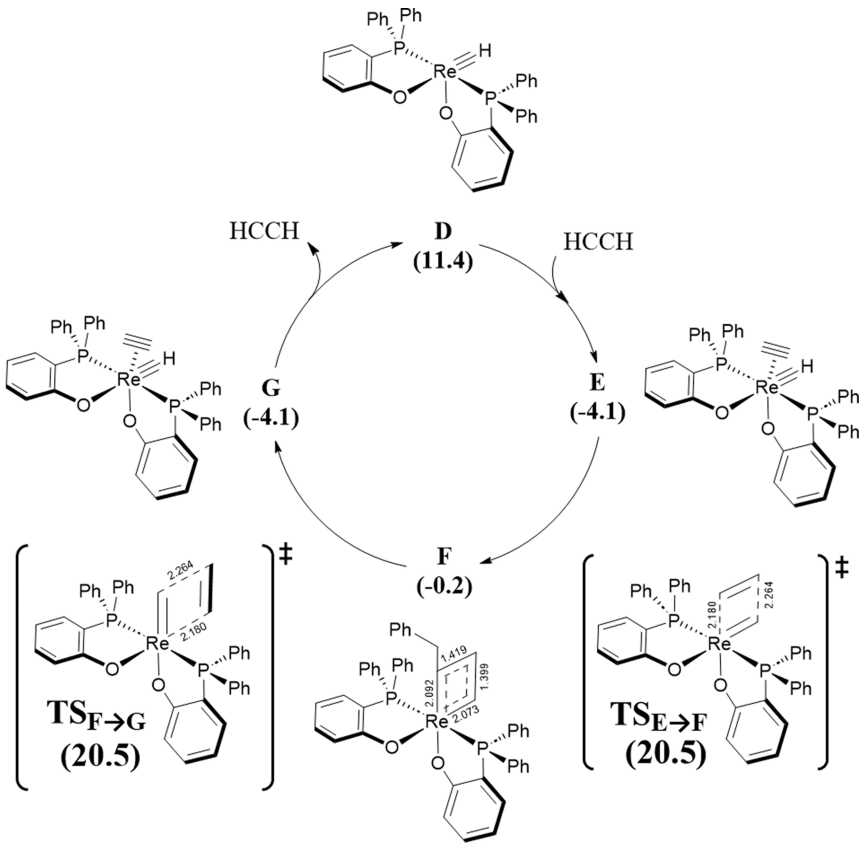

Figure 3. Re-based catalyzed pathway for alkyne metathesis (relative Gibbs free energies in kcal/mol with respect to **R**, and selected distances in Å).

black in Figure 2. Thermodynamically, the latter is 8.5 kcal/mol more stable than **Δ-*cis*A**, thus placed 4.9 kcal/mol below the reference complex **R**. More importantly, it can efficiently catalyze the reaction (Figure 2), since $\Delta\Delta G^{\ddagger}_{TSB\rightarrow C}$ = 17.7 kcal/mol, clearly favoring the **Λ** based one. Structurally the difference is that the two phosphorus atoms are placed *cis* in **Δ-*cis*A** and trans in **Λ-*cis*A**. Ignoring the axis with the coordinated alkyne, the average of the two remaining P−Re−P and C−Re−O axes for **Λ-*cis*A** is 166.0°, 2.0 closer to linearity than for **Δ-*cis*A**, across its P−Re−O and C−Re−O axes. In addition, although it may seem contradictory, the axis P−Re−P where the alkyne in **Λ-*cis*A** is inserted is 157.3° while it is 161.1° in the P−Re−O for **Δ-*cis*A**, that is, it being more difficult in the latter case to accommodate the alkyne, especially with sterically hindered substituents. In fact, the coordination of the alkyne is more symmetrical maintaining better the κ^2 coordination for **Λ-*cis*A** with Re−C bond distances of 2.143 and 2.158 Å than for **Δ-*cis*A** (2.223 and 2.150 Å). The difference in stability of both isomers can also be rationalized by analyzing the frontier molecular orbitals (see Figures S1 and S2 in the SI). In **Λ-*cis*A**, no alkyne atomic orbital contribution is present to form the HOMO and LUMO while an orbital node is present in **Δ-*cis*A** LUMO in the region between Re and an alkyne carbon atom. As a consequence, one alkyne carbon is more negatively charged than the other in **Δ-*cis*A**, as shown by the NAO-obtained atomic charges (q_{C1} = −0.215 vs q_{C2} = −0.174). In contrast, the difference in atomic charge in **Λ-*cis*A** (q_{C1} = −0.225 vs q_{C2} = −0.228) is not as large, making the complex more stable. Furthermore, apart from the series of structural factors (distortion in coordination of acetylene, steric repulsion between phosphine groups, etc.) that contribute to the relative stability favoring **Λ-*cis*A**, the HOMO−LUMO gap is lower in **Λ-*cis*A** than in **Δ-*cis*A** (102.0 kcal/mol for **Λ-*cis*A** vs 103.7 kcal/mol for **Δ-*cis*A**). The nonplanarity of intermediate **B** can be rationalized by the HOMO and LUMO shapes. By visual inspection of the HOMO of **Δ-*cis*A**, one observes that the orbital lobes around the Re alkylidyne bond form an angle of 135° with the Re−P bond if visualized along the Re alkylidyne bond (top view in the SI). Hence, when the alkyne rotates to form rhenacyclobutadiene species **B**, the best overlap between the HOMO lobe centered at $C_{alkylidyne}$ and the LUMO lobe centered at C1 will result in a nonplanar rhenacyclobutadiene. Then, the nonplanarity of **B** influences how the metal interacts with the neighboring atoms. For its analysis, we used the Mayer bond orders (MBOs).[43] While the MBO of the Re−$C_{alkylidyne}$ bond (MBO = 1.019 in **Δ-*cis*B** vs MBO = 1.787 in **Δ-*cis*A**) and MBO C1−C2 (MBO = 1.348 in **Δ-*cis*B** vs MBO = 2.176 in **Δ-*cis*A**) are lower than those corresponding ones to **Λ-*cis*A**,[44] the C1−$C_{alkylidyne}$ bond is far from being the ideal double bond (MBO = 1.130 in **Δ-*cis*B**).[45] In contrast, starting from **Λ-*cis*A**, the reaction can proceed without the need to overcome a high activation energy barrier. Indeed, although intermediate **Λ-*cis*B** is formed after overcoming a higher activation energy barrier (23.9 kcal/mol, thus 3.9 kcal/mol more than the previous case) mainly due to the higher stabilization of **Λ-*cis*A**, the formation of intermediate **C** (ΔG = 8.1 kcal/mol) becomes kinetically feasible through **TS$_{B\rightarrow C}$** ($\Delta G^{\ddagger}$ = 26.8 kcal/mol). The lower required energy is due to the difference in MBO in **Λ-*cis*B** with respect to **Δ-*cis*B**. Particularly, the planarity of the rhenacyclobutadiene leads to a stronger C1−$C_{alkylidyne}$ bond (MBO = 1.356 in **Λ-*cis*B** vs MBO

https://doi.org/10.1021/acs.inorgchem.3c04235
Inorg. Chem. 2024, 63, 5842−5851

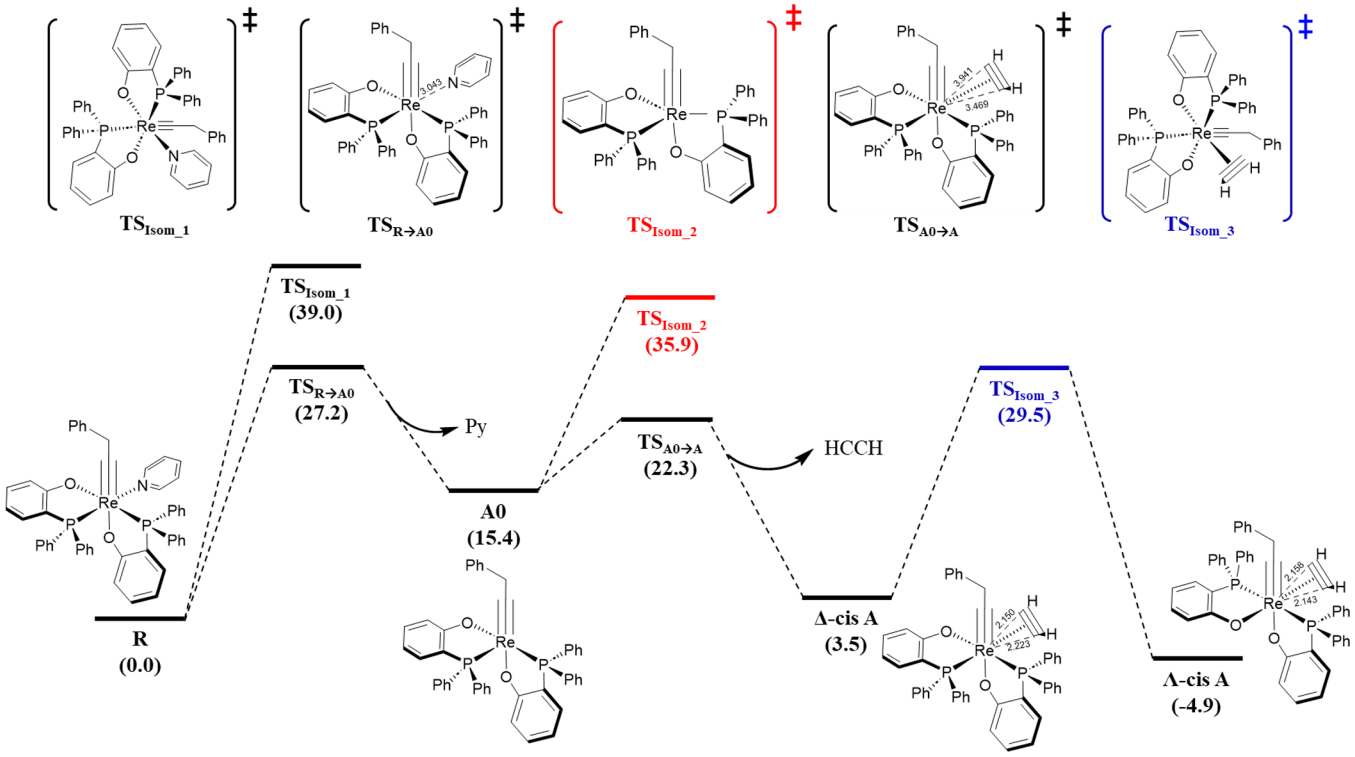

Figure 4. Re-based catalyzed pathway of the isomerization (relative Gibbs free energies are given in kcal/mol with respect to **R**).

= 1.787 in **Δ-*cis*B**) and weaker Re−$C_{alkylidyne}$ (MBO = 0.701 in **Λ-*cis*B** vs MBO = 1.019 in **Δ-*cis*B**) and C1−C2 (MBO = 1.314 in **Λ-*cis*B** vs MBO = 1.348 in **Δ-*cis*B**).

From **C** a molecule of benzyl acetylene is released into the solution forming intermediate **D** (ΔG = 11.4 kcal/mol). The newly formed **D** bears a vacant site, and it can easily be coordinated by acetylene to form the η^2-acetylene complex **E** (ΔG = −4.1 kcal/mol). Above with **A**, the reaction proceeds with a cycloaddition step to form the rhenacyclobutadiene **F** (ΔG = −0.2 kcal/mol) followed by a cycloelimination step (Figure 4). However, unlike what happens with **A**, **TS**$_{E→F}$, and **TS**$_{F→G}$ are isoenergetic ($\Delta G^{‡}$ = 20.5 kcal/mol) while **E** is symmetrical. Finally, intermediate **G** (ΔG = −4.1 kcal/mol) is formed and releases an acetylene molecule into the solution, forming again the unstable intermediate **D** (ΔG = 11.4 kcal/mol) ready to react with another acetylene molecule and continuing with the catalytic cycle (Figure 3). Once it was established that **Λ-*cis*A** kinetically favors the reaction, the isomerization mechanism from the Δ-*cis* isomer to a Λ-*cis* one has been studied (Figure 4). Isomerization can occur once the pyridine has left, forming **A0** or via an intramolecular twisted transition state apart from **R** or **A** without breaking any bond. Indeed, **R** can isomerize via a Rây−Dutt twisted **TS**$_{Isom\_1}$ ($\Delta G^{‡}$ = 39.0 kcal/mol).[46] On the other hand, isomerization is more favored through a trigonal bipyramidal **TS**$_{Isom\_2}$ ($\Delta G^{‡}$ = 35.9 kcal/mol). In fact, the dissociation of the pyridine allows the rotation along the C−Re−O axis of one PO ligand, since the dissociation of pyridine frees up enough space to make that rotation feasible. To a lesser extent, but not least, the direct isomerization of **Δ-*cis*A** to **Λ-*cis*A** was analyzed. This isomerization mechanism is kinetically much more favored than the previous ones that occur via a Rây−Dutt twisted **TS**$_{Isom\_3}$ ($\Delta G^{‡}$ = 29.5 kcal/mol).

By applying the Kozuch−Shaik energetic span model theory to our catalytic cycle,[47] an overall energetic span δE of 34.4 kcal/mol is obtained, with **TS**$_{Isom\_3}$ being the TOF-determining transition state (TDTS) and **Λ-*cis*A** the TOF-determining intermediate (TDI). Once the TDTS and the TDI species were identified, a series of catalysts (Table 1, entries 1−7) were analyzed tuning the steric and electronic properties of the PO ligands. As shown in Table 1, the presence of a more electron-withdrawing phosphine (entry 2) does not influence the reactivity as much because the resulting stabilization of **TS**$_{Isom\_3}$ ($\Delta\Delta G^{‡}$ = −1.7 kcal/mol) is compensated by the stabilization of **Λ-*cis*A** ($\Delta\Delta G$ = −1.3 kcal/mol), while the presence of more electron-donating groups (entries 3 and 4) leads to slightly higher δE due to the destabilization of **TS**$_{Isom\_3}$ ($\Delta\Delta G^{‡}$ = +0.8 kcal/mol) such as in entry 3 or a stabilization of **Λ-*cis*A** ($\Delta\Delta G$ = −1.3 kcal/mol) such as in entry 4. Furthermore, a CF_3 group in para to the oxygen (entry 5) destabilizes **TS**$_{Isom\_3}$, resulting in a larger δE (37.2 vs 34.4 kcal/mol without substituents), whereas an

Table 1. Ligand Substitution Scope (See Scheme 2b) for the Alkyne Metathesis Reaction Studied[a]

entry	R_1	R_2	Λ-*cis* A	TS$_{Isom_3}$	δE
1[a]	H	Ph	−4.9	29.5	34.4
2[a]	H	(*p*-CF_3)Ph	−6.2	27.8	34.0
3[a]	H	(*p*-OMe)Ph	−4.9	30.3	35.2
4	H	(*p*-Me)Ph	−6.5	29.0	35.5
5[a]	CF_3	Ph	−4.6	32.6	37.2
6	Me	Ph	−4.5	30.2	34.7
7[a]	H	Cy	−4.4	26.7	31.1
8	H	Me	−5.4	27.4	32.8

[a]Gibbs energies in kcal/mol. a = catalyst tested experimentally by Jia et al.

https://doi.org/10.1021/acs.inorgchem.3c04235
Inorg. Chem. 2024, 63, 5842−5851

electron-donating group such as Me (entry 6) does not influence much the reactivity ($\Delta\delta E$ = +0.3 kcal/mol). On the other hand, the presence of an electron-donating phosphine (entries 7 and 8) predicts better catalysts due to a lower δE (31.1 and 32.8 kcal/mol for **7** and **8** vs 34.4 kcal/mol for **1**), resulting from the stabilization of species $\mathbf{TS_{Isom\_3}}$. Experimentally, Jia and co-workers analyzed the kinetics of the homometathesis using 1-methoxy-4-(1-propyn-1-yl)benzene and catalysts **1**−**3**, **5**, and **7**.[31] Similar kinetics were obtained for catalysts **1**−**3** and **5**, while **7** was the best catalyst. Although we modeled the reaction using acetylene as the reactant, our computational results show similar δEs for catalysts **1**−**3** and **5** (34.4, 34.0, 35.2, and 37.2 kcal/mol, respectively). At the same time, the δE for **7** is lowered to 31.1 kcal/mol. With this, our results nicely fit with the experimental evidence, as catalysts present similar kinetics, except for the catalyst bearing cyclohexylphosphine, which in both studies presented faster catalysis.

Overall, no clear trends are extracted solely on the basis of modifying the electronic character (withdrawing vs donating) of the substituents. Instead, and as already pinpointed in the literature,[48] the tris-chelate metal complexes isomerization is influenced by the bite angle of the ligand. First, the stability of **Λ-*cis*A** has been correlated with one O−Re−P bite angle of **Λ-*cis*A** (R^2 = 0.890). Simultaneously, δE presents a rather large linear correlation with the same bite angle (R^2 = 0.759), the one with the alkyne−Re−$C_{alkylidyne}$ angle in between (R^2 = 0.842, R_2 = Cy excluded from correlation). Considering the two variables together, the correlation improves (R^2 = 0.784). The graphical representation of the linear regressions is provided in Figures S6−S8. Again, the influence of this angle can be rationalized by visual inspection of the molecular orbitals of **Λ-*cis*A**. The HOMO is delocalized over the O−Re−P bite angle; meanwhile, the alkyne−Re−$C_{alkylidyne}$ is distorted due to the repulsion between the π systems electron cloud of alkyne and alkylidyne.

Finally, the effect of substituents on the alkyne has been evaluated in a predictive way.[33,49] In the case of using propyne instead of acetylene, $\mathbf{TS_{Isom\_3}}$ is destabilized (31.4 vs 29.5 kcal/mol with acetylene), and also **Λ-*cis*A** results in destabilization (1.7 vs −4.9 kcal/mol) due to the larger steric hindrance. The P−Re−P angle is distorted increasing the steric hindrance of the substituents of the simple acetylene, going from 157.3 to 155.2° for propyne. Going to an analysis of the steric hindrance using the steric maps of Cavallo and co-workers,[50] it was found that at the midpoint of the two carbons of the alkyne entering the intermediate **Λ-*cis*A**, the $\%V_{Bur}$ increases from 65.3 to 71.5% (Figure 5). This is logical, but the difference should have been smaller due to the distortion of the P−Re−P angle to accommodate the alkyne mentioned above. However, a full understanding of the substituent effect is required for further studies.

CONCLUSIONS

In summary, our study presents a comprehensive mechanistic investigation of Re(V)-based alkyne metathesis, building upon the experimental findings reported by Jia and co-workers.[31] DFT calculations revealed that the reaction initiates with the dissociation of the pyridine, followed by the entry of an alkyne molecule via a stepwise mechanism. However, the reaction necessitates an isomerization process, as the activation pathway in the retrocycloaddition step is kinetically impossible under the experimental conditions (44.5 kcal/mol). Interestingly, the reaction can effectively proceed through the **Λ-*cis*A** stereoisomer without a prohibitive overall activation energy barrier.

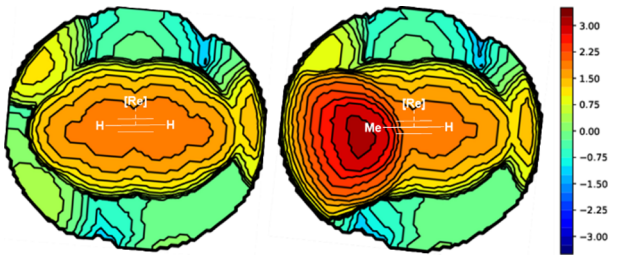

Figure 5. Steric maps of species **Λ-*cis*A** for the alkynes: (a) acetylene and (b) propyne, with the corresponding $\%V_{Bur}$ values on the *xy* plane (using the two carbon atoms of the alkyne as center, with a radius of 3.5 Å and with the *z*-axis defined by the metal; the *xy* plane is perpendicular to the *z*-axis and contains both carbon atoms of the alkyne, including the H atoms). Isocontour curves are given in Å.

Further exploration of all possible isomerization pathways revealed that while the isomerization becomes hindered when the pyridine is bonded, the process is significantly facilitated upon its exchange with an alkyne. With this, $\mathbf{TS_{Isom\_3}}$ results being the reaction TDTS. Experimental evidence suggests that the TDTS is the pyridine dissociation, and although most of the DFT calculations are performed with the simplified acetylene, our results corroborate well with the reported experimental kinetics. In fact, aryl phosphines provide similar kinetics, and the cyclohexylphosphine catalyst is the best catalyst. It is worth mentioning that the faster the pyridine leaves, the faster the catalyst can isomerize.

Moreover, our results revealed that the isomerization seems to depend on the phosphine-phenolate bite angles in **Λ-*cis*A**, whereas adding substituents on acetylene seems destabilizing slightly $\mathbf{TS_{Isom\_3}}$ and much more **Λ-*cis*A** due to the higher steric hindrance between the methyl substituent and the phenyl phosphine.

ASSOCIATED CONTENT

Supporting Information

The Supporting Information is available free of charge at https://pubs.acs.org/doi/10.1021/acs.inorgchem.3c04235.

Coordinates for all reactants, intermediates, and transition states (XYZ)

Frontier molecular orbital analysis of selected species, 3D-view of selected transition states, relative energies and selected angles for the crucial species of the ligand substitution scope, and plots of the linear correlations attempted in the study (PDF)

AUTHOR INFORMATION

Corresponding Authors

Martí Gimferrer − *Institut für Physikalische Chemie, Georg-August Universität Göttingen, Göttingen 37077, Germany;* orcid.org/0000-0001-5222-2201; Email: marti.gimferrerandres@uni-goettingen.de

Lucia Caporaso − *Dipartimento di Chimica e Biologia, Università di Salerno, Fisciano 84084, Italy; CIRCC, Interuniversity Consortium Chemical Reactivity and Catalysis, Bari 70126, Italy;* orcid.org/0000-0001-6623-3315; Email: lcaporaso@unisa.it

Albert Poater − *Institut de Química Computacional i Catàlisi, Departament de Química, Universitat de Girona, Girona*

https://doi.org/10.1021/acs.inorgchem.3c04235
Inorg. Chem. 2024, 63, 5842−5851

17003 Catalonia, Spain; orcid.org/0000-0002-8997-2599; Email: albert.poater@udg.edu

Author

Michele Tomasini − *Institut de Química Computacional i Catàlisi, Departament de Química, Universitat de Girona, Girona 17003 Catalonia, Spain; Dipartimento di Chimica e Biologia, Università di Salerno, Fisciano 84084, Italy;* orcid.org/0000-0002-1366-1401

Complete contact information is available at: https://pubs.acs.org/10.1021/acs.inorgchem.3c04235

Notes

The authors declare no competing financial interest.

■ ACKNOWLEDGMENTS

A.P. is a Serra Húnter Fellow and received ICREA Academia Prize 2019. We thank the Spanish Ministerio de Ciencia e Innovación for project PID2021-127423NB-I00 and the Generalitat de Catalunya for project 2021SGR623. M.G. thanks being partially funded by the Deutsche Forschungsgemeinschaft (DFG, German Research Foundation)—217133147/SFB 1073, project C03.

■ REFERENCES

(1) Haibach, M. C.; Kundu, S.; Brookhart, M.; Goldman, A. S. Alkane Metathesis by Tandem Alkane-Dehydrogenation−Olefin-Metathesis Catalysis and Related Chemistry. *Acc. Chem. Res.* **2012**, *45*, 947−958.

(2) Bailey, B. C.; Schrock, R. R.; Kundu, S.; Goldman, A. S.; Huang, Z.; Brookhart, M. Evaluation of molybdenum and tungsten metathesis catalysts for homogeneous tandem alkane metathesis. *Organometallics* **2009**, *28*, 355−360.

(3) (a) Hérisson, P. J. L.; Chauvin, Y. Catalyse de transformation des oléfines par les complexes du tungstène. II. Télomérisation des oléfines cycliques en présence d'oléfines acycliques. *Die Makromol. Chem.* **1971**, *141*, 161−176. (b) Chauvin, Y. Olefin Metathesis: The Early Days (Nobel Lecture). *Angew. Chem., Int. Ed.* **2006**, *45*, 3740−3747.

(4) (a) Schrock, R. R. Multiple Metal-Carbon Bonds for Catalytic Metathesis Reactions (Nobel Lecture). *Angew. Chem., Int. Ed.* **2006**, *45*, 3748−3759. (b) Grubbs, R. H. Olefin-Metathesis Catalysts for the Preparation of Molecules and Materials (Nobel Lecture). *Angew. Chem., Int. Ed.* **2006**, *45*, 3760−3765.

(5) (a) Grubbs, R. H.; Wenzel, A. G.; O'Leary, D. J.; Khosravi, E. *Handbook of Metathesis*; John Wiley & Sons, 2015. (b) Montgomery, T. P.; Johns, A. M.; Grubbs, R. H. Recent Advancements in Stereoselective Olefin Metathesis Using Ruthenium Catalysts. *Catalysts* **2017**, *7*, 87 DOI: 10.3390/catal7030087. (c) Herbert, M. B.; Grubbs, R. H. Z-Selective Cross Metathesis with Ruthenium Catalysts: Synthetic Applications and Mechanistic Implications. *Angew. Chem., Int. Ed.* **2015**, *54*, 5018−5024. (d) Fustero, S.; Simón-Fuentes, A.; Barrio, P.; Haufe, G. Olefin Metathesis Reactions with Fluorinated Substrates, Catalysts, and Solvents. *Chem. Rev.* **2015**, *115*, 871−930. (e) Schrock, R. R. Synthesis of stereoregular polymers through ring-opening metathesis polymerization. *Acc. Chem. Res.* **2014**, *47*, 2457−2466.

(6) (a) Fürstner, A. The Ascent of Alkyne Metathesis to Strategy-Level Status. *J. Am. Chem. Soc.* **2021**, *143*, 15538−15555. (b) Lee, D.; Volchkov, I.; Yun, S. Y. Alkyne Metathesis. *Org. React.* **2020**, *102*, 613−931.

(7) Ehrhorn, H.; Tamm, M. Well-Defined Alkyne Metathesis Catalysts: Developments and Recent Applications. *Chem.—Eur. J.* **2019**, *25*, 3190−3208.

(8) (a) Yiannakas, E.; Grimes, M. I.; Whitelegge, J. T.; Fürstner, A.; Hulme, A. N. An Alkyne-Metathesis-Based Approach to the Synthesis of the Anti-Malarial Macrodiolide Samroiyotmycin A. *Angew. Chem., Int. Ed.* **2021**, *60*, 18504−18508. (b) Löffler, L. E.; Wirtz, C.; Fürstner, A. Collective Total Synthesis of Casbane Diterpenes: One Strategy, Multiple Targets. *Angew. Chem., Int. Ed.* **2021**, *60*, 5316−5322. (c) Schulthoff, S.; Hamilton, J. Y.; Heinrich, M.; Kwon, Y.; Wirtz, C.; Fürstner, A. The Formosalides: Structure Determination by Total Synthesis. *Angew. Chem., Int. Ed.* **2021**, *60*, 446−454. (d) Meng, Z.; Spohr, S. M.; Tobegen, S.; Farès, C.; Fürstner, A. A Unified Approach to Polycyclic Alkaloids of the Ingenamine Estate: Total Syntheses of Keramaphidin B, Ingenamine, and Nominal Njaoamine I. *J. Am. Chem. Soc.* **2021**, *143*, 14402−14414. (e) Meng, Z.; Fürstner, A. Total Synthesis Provides Strong Evidence: Xestocyclamine A is the Enantiomer of Ingenamine. *J. Am. Chem. Soc.* **2020**, *142*, 11703−11708.

(9) (a) Kiel, G. R.; Bay, K. L.; Samkian, A. E.; Schuster, N. J.; Lin, J. B.; Handford, R. C.; Nuckolls, C.; Houk, K. N.; Tilley, T. D. Expanded Helicenes as Synthons for Chiral Macrocyclic Nanocarbons. *J. Am. Chem. Soc.* **2020**, *142*, 11084−11091. (b) Jiang, X.; Laffoon, J. D.; Chen, D.; Pérez-Estrada, S.; Danis, A. S.; Rodríguez-López, J.; Garcia-Garibay, M. A.; Zhu, J.; Moore, J. S. Kinetic Control in the Synthesis of a Möbius Tris((ethynyl)[5]helicene) Macrocycle Using Alkyne Metathesis. *J. Am. Chem. Soc.* **2020**, *142*, 6493−6498. (c) Cencer, M. M.; Greenlee, A. J.; Moore, J. S. Quantifying Error Correction through a Rule-Based Model of Strand Escape from an [n]-Rung Ladder. *J. Am. Chem. Soc.* **2020**, *142*, 162−168. (d) Ortiz, M.; Cho, S.; Niklas, J.; Kim, S.; Poluektov, O. G.; Zhang, W.; Rumbles, G.; Park, J. Through-Space Ultrafast Photoinduced Electron Transfer Dynamics of a C_{70}-Encapsulated Bisporphyrin Covalent Organic Polyhedron in a LowDielectric Medium. *J. Am. Chem. Soc.* **2017**, *139*, 4286−4289. (e) Lee, S.; Chénard, E.; Gray, D. L.; Moore, J. S. Synthesis of Cycloparaphenyleneacetylene via Alkyne Metathesis: C70 Complexation and Copper-Free Triple Click Reaction. *J. Am. Chem. Soc.* **2016**, *138*, 13814−13817. (f) Lee, S.; Yang, A.; Moneypenny, T. P., 2nd; Moore, J. S. Kinetically Trapped Tetrahedral Cages via Alkyne Metathesis. *J. Am. Chem. Soc.* **2016**, *138*, 2182−2185. (g) Wang, Q.; Yu, C.; Zhang, C.; Long, H.; Azarnoush, S.; Jin, Y.; Zhang, W. Dynamic covalent synthesis of aryleneethynylene cages through alkyne metathesis: dimer, tetramer, or interlocked complex? *Chem. Sci.* **2016**, *7*, 3370−3376. (h) Wang, Q.; Yu, C.; Long, H.; Du, Y.; Jin, Y.; Zhang, W. Solution-phase dynamic assembly of permanently interlocked aryleneethynylene cages through alkyne metathesis. *Angew. Chem., Int. Ed.* **2015**, *54*, 7550−7554. (i) Wang, Q.; Zhang, C.; Noll, B. C.; Long, H.; Jin, Y.; Zhang, W. A Tetrameric Cage with D2h Symmetry through Alkyne Metathesis. *Angew. Chem., Int. Ed.* **2014**, *53*, 10663−10667. (j) Zhang, C.; Wang, Q.; Long, H.; Zhang, W. A highly C_{70} selective shape-persistent rectangular prism constructed through onestep alkyne metathesis. *J. Am. Chem. Soc.* **2011**, *133*, 20995−21001. (k) Huang, S.; Lei, Z.; Jin, Y.; Zhang, W. By-design molecular architectures via alkyne metathesis. *Chem. Sci.* **2021**, *12*, 9591−9606.

(10) (a) von Kugelgen, S.; Piskun, I.; Griffin, J. H.; Eckdahl, C. T.; Jarenwattananon, N. N.; Fischer, F. R. Templated Synthesis of EndFunctionalized Graphene Nanoribbons through Living Ring-Opening Alkyne Metathesis Polymerization. *J. Am. Chem. Soc.* **2019**, *141*, 11050−11058. (b) Jeong, H.; von Kugelgen, S.; Bellone, D.; Fischer, F. R. Regioselective Termination Reagents for Ring-Opening Alkyne Metathesis Polymerization. *J. Am. Chem. Soc.* **2017**, *139*, 15509−15514. (c) von Kugelgen, S.; Sifri, R.; Bellone, D.; Fischer, F. R. Regioselective Carbyne Transfer to Ring-Opening Alkyne Metathesis Initiators Gives Access to Telechelic Polymers. *J. Am. Chem. Soc.* **2017**, *139*, 7577−7585. (d) von Kugelgen, S.; Bellone, D. E.; Cloke, R. R.; Perkins, W. S.; Fischer, F. R. Initiator Control of Conjugated Polymer Topology in Ring-Opening Alkyne Metathesis Polymerization. *J. Am. Chem. Soc.* **2016**, *138*, 6234−6239.

(11) (a) Fürstner, A. Lessons from Natural Product Total Synthesis: Macrocyclization and Postcyclization Strategies. *Acc. Chem. Res.* **2021**, *54*, 861−874. (b) Yang, H.; Jin, Y.; Du, Y.; Zhang, W. Application of alkyne metathesis in polymer synthesis. *J. Mater. Chem. A* **2014**, *2*, 5986−5993.

(12) (a) Zhang, W.; Moore, J. S. Synthesis of Poly(2,5-thienyleneethynylene)s by Alkyne Metathesis. *Macromolecules* **2004**, *37*, 3973−3975. (b) Bunz, U. H. F. Poly(pphenyleneethynylene)s by Alkyne Metathesis. *Acc. Chem. Res.* **2001**, *34*, 998−1010. (c) Brizius, G.; Pschirer, N. G.; Steffen, W.; Stitzer, K.; zur Loye, H.-C.; Bunz, U. H. F. Alkyne Metathesis with Simple Catalyst Systems: Efficient Synthesis of Conjugated Polymers Containing Vinyl Groups in Main or Side Chain. *J. Am. Chem. Soc.* **2000**, *122*, 12435−12440.

(13) (a) Wengrovius, J. H.; Sancho, J.; Schrock, R. R. Metathesis of acetylenes by tungsten(VI)-alkylidyne complexes. *J. Am. Chem. Soc.* **1981**, *103*, 3932−3934. (b) Sancho, J.; Schrock, R. R. Acetylene metathesis by tungsten(VI) alkylidyne complexes. *J. Mol. Catal.* **1982**, *15*, 75−79. (c) McCullough, L. G.; Schrock, R. R. *Multiple metal-carbon bonds*. (d) Metathesis of acetylenes by molybdenum(VI) alkylidyne complexes. *J. Am. Chem. Soc.* **1984**, *106*, 4067−4068 (e) McCullough, L. G.; Schrock, R. R.; Dewan, J. C.; Murdzek, J. C. Preparation of trialkoxymolybdenum (VI) alkylidyne complexes, their reactions with acetylenes, and the X-ray structure of $Mo[C_3(CMe_3)_2]$-$[OCH\text{-}(CF_3)_2]_2(C_5H_5N)_2$. *J. Am. Chem. Soc.* **1985**, *107*, 5987−5998. (f) Schrock, R. R. Alkyne metathesis by molybdenum and tungsten alkylidyne complexes. *Chem. Commun.* **2013**, *49*, 5529−5531. (g) Schrock, R. R. High Oxidation State Multiple Metal−Carbon Bonds. *Chem. Rev.* **2002**, *102*, 145−180. (h) Schrock, R. R. High-oxidation-state molybdenum and tungsten alkylidyne complexes. *Acc. Chem. Res.* **1986**, *19*, 342−348.

(14) Pennella, F.; Banks, R. L.; Bailey, G. C. Disproportionation of alkynes. *Chem. Commun.* **1968**, 1548−1549.

(15) (a) Mortreux, A.; Blanchard, M. Metathesis of alkynes by a molybdenum hexacarbonyl-resorcinol catalyst. *J. Chem. Soc., Chem. Commun.* **1974**, 786−787. (b) Bencheick, A.; Petit, M.; Mortreux, A.; Petit, F. New active and selective catalysts for homogeneous metathesis of disubstituted alkynes. *J. Mol. Catal.* **1982**, *15*, 93−101.

(16) (a) Haberlag, B.; Freytag, M.; Daniliuc, C. G.; Jones, P. G.; Tamm, M. Efficient metathesis of terminal alkynes. *Angew. Chem., Int. Ed.* **2012**, *51*, 13019−13022. (b) Ehrhorn, H.; Bockfeld, D.; Freytag, M.; Bannenberg, T.; Kefalidis, C. E.; Maron, L.; Tamm, M. Studies on Molybdena- and Tungstenacyclobutadiene Complexes Supported by Fluoroalkoxy Ligands as Intermediates of Alkyne Metathesis. *Organometallics* **2019**, *38*, 1627−1639. (c) Bittner, C.; Ehrhorn, H.; Bockfeld, D.; Brandhorst, K.; Tamm, M. Tuning the Catalytic Alkyne Metathesis Activity of Molybdenum and Tungsten 2,4,6-Trimethylbenzylidyne Complexes with Fluoroalkoxide Ligands $OC(CF_3)$-nMe_3−n (n = 0−3). *Organometallics* **2017**, *36*, 3398−3406.

(17) (a) Bindl, M.; Stade, R.; Heilmann, E. K.; Picot, A.; Goddard, R.; Fürstner, A. Molybdenum nitride complexes with Ph_3SiO ligands are exceedingly practical and tolerant precatalysts for alkyne metathesis and efficient nitrogen transfer agents. *J. Am. Chem. Soc.* **2009**, *131*, 9468−9470. (b) Heppekausen, J.; Stade, R.; Goddard, R.; Fürstner, A. Practical new silyloxy-based alkyne metathesis catalysts with optimized activity and selectivity profiles. *J. Am. Chem. Soc.* **2010**, *132*, 11045−11057. (c) Heppekausen, J.; Stade, R.; Kondoh, A.; Seidel, G.; Goddard, R.; Fürstner, A. Optimized synthesis, structural investigations, ligand tuning and synthetic evaluation of silyloxy-based alkyne metathesis catalysts. *Chem.—Eur. J.* **2012**, *18*, 10281−10299. (d) Schnabel, T. M.; Melcher, D.; Brandhorst, K.; Bockfeld, D.; Tamm, M. Unraveling the Mechanism of 1,3-Diyne Cross-Metathesis Catalyzed by Silanolate-Supported Tungsten Alkylidyne Complexes. *Chem.—Eur. J.* **2018**, *24*, 9022−9032. (e) Lysenko, S.; Volbeda, J.; Jones, P. G.; Tamm, M. Catalytic metathesis of conjugated diynes. *Angew. Chem., Int. Ed.* **2012**, *51*, 6757−6761. (f) Lysenko, S.; Haberlag, B.; Daniliuc, C. G.; Jones, P. G.; Tamm, M. Efficient Catalytic Alkyne Metathesis with a Tri(tert-butoxy)silanolate-Supported Tungsten Benzylidyne Complex. *ChemCatChem.* **2011**, *3*, 115−118.

(18) (a) Beer, S.; Hrib, C. G.; Jones, P. G.; Brandhorst, K.; Grunenberg, J.; Tamm, M. Efficient room-temperature alkyne metathesis with well-defined imidazolin-2-iminato tungsten alkylidyne complexes. *Angew. Chem., Int. Ed.* **2007**, *46*, 8890−8894. (b) Beer, S.; Brandhorst, K.; Hrib, C. G.; Wu, X.; Haberlag, B.; Grunenberg, J.; Jones, P. G.; Tamm, M. Experimental and Theoretical Investigations of Catalytic Alkyne Cross-Metathesis with Imidazolin-2-iminato Tungsten Alkylidyne Complexes. *Organometallics* **2009**, *28*, 1534−1545. (c) Haberlag, B.; Wu, X.; Brandhorst, K.; Grunenberg, J.; Daniliuc, C. G.; Jones, P. G.; Tamm, M. Preparation of imidazolin-2-iminato molybdenum and tungsten benzylidyne complexes: a new pathway to highly active alkyne metathesis catalysts. *Chem.—Eur. J.* **2010**, *16*, 8868−8877.

(19) Melcher, D.; Àrias, Ò.; Freytag, M.; Jones, P. G.; Tamm, M. Synthesis of Alkyne Metathesis Catalysts from Tris(dimethylamido) tungsten Precursors. *Eur. J. Inorg. Chem.* **2020**, *2020*, 4454−4464.

(20) (a) Estes, D. P.; Gordon, C. P.; Fedorov, A.; Liao, W.-C.; Ehrhorn, H.; Bittner, C.; Zier, M. L.; Bockfeld, D.; Chan, K. W.; Eisenstein, O.; Raynaud, C.; Tamm, M.; Copéret, C. Molecular and Silica-Supported Molybdenum Alkyne Metathesis Catalysts: Influence of Electronics and Dynamics on Activity Revealed by Kinetics, SolidState NMR, and Chemical Shift Analysis. *J. Am. Chem. Soc.* **2017**, *139*, 17597−17607. (b) Zier, M. L.; Colombel-Rouen, S.; Ehrhorn, H.; Bockfeld, D.; Trolez, Y.; Mauduit, M.; Tamm, M. Catalytic Alkyne and Diyne Metathesis with Mixed Fluoroalkoxy-Siloxy Molybdenum Alkylidyne Complexes. *Organometallics* **2021**, *40*, 2008−2015.

(21) (a) Groos, J.; Hauser, P. M.; Koy, M.; Frey, W.; Buchmeiser, M. R. Highly Reactive Cationic Molybdenum Alkylidyne N-Heterocyclic Carbene Catalysts for Alkyne Metathesis. *Organometallics* **2021**, *40*, 1178−1184. (b) Elser, I.; Groos, J.; Hauser, P. M.; Koy, M.; van der Ende, M.; Wang, D.; Frey, W.; Wurst, K.; Meisner, J.; Ziegler, F.; Kästner, J.; Buchmeiser, M. R. Molybdenum and Tungsten Alkylidyne Complexes Containing Mono-, Bi-, and Tridentate N-Heterocyclic Carbenes. *Organometallics* **2019**, *38*, 4133−4146. (c) Koy, M.; Elser, I.; Meisner, J.; Frey, W.; Wurst, K.; Kästner, J.; Buchmeiser, M. R. High Oxidation State Molybdenum N -Heterocyclic Carbene Alkylidyne Complexes: Synthesis, Mechanistic Studies, and Reactivity. *Chem.—Eur. J.* **2017**, *23*, 15484−15490.

(22) (a) Zhang, W.; Kraft, S.; Moore, J. S. Highly active trialkoxymolybdenum(VI) alkylidyne catalysts synthesized by a reductive recycle strategy. *J. Am. Chem. Soc.* **2004**, *126*, 329−335. (b) Zhang, W.; Kraft, S.; Moore, J. S. A reductive recycle strategy for the facile synthesis of molybdenum(VI) alkylidyne catalysts for alkyne metathesis. *Chem. Commun.* **2003**, 832−833.

(23) (a) Jyothish, K.; Zhang, W. Introducing a podand motif to alkyne metathesis catalyst design: a highly active multidentate molybdenum(VI) catalyst that resists alkyne polymerization. *Angew. Chem., Int. Ed.* **2011**, *50*, 3435−3438. (b) Jyothish, K.; Wang, Q.; Zhang, W. Highly Active Multidentate Alkyne Metathesis Catalysts: Ligand-Activity Relationship and Their Applications in Efficient Synthesis of Porphyrin-Based Aryleneethynylene Polymers. *Adv. Synth. Catal.* **2012**, *354*, 2073−2078. (c) Yang, H.; Liu, Z.; Zhang, W. Multidentate Triphenolsilane-Based Alkyne Metathesis Catalysts. *Adv. Synth. Catal.* **2013**, *355*, 885−890. (d) Du, Y.; Yang, H.; Zhu, C.; Ortiz, M.; Okochi, K. D.; Shoemaker, R.; Jin, Y.; Zhang, W. Highly Active Multidentate Ligand-Based Alkyne Metathesis Catalysts. *Chem.—Eur. J.* **2016**, *22*, 7959−7963.

(24) (a) Hillenbrand, J.; Leutzsch, M.; Fürstner, A. Molybdenum Alkylidyne Complexes with Tripodal Silanolate Ligands: The Next Generation of Alkyne Metathesis Catalysts. *Angew. Chem., Int. Ed.* **2019**, *58*, 15690−15696. (b) Hillenbrand, J.; Leutzsch, M.; Yiannakas, E.; Gordon, C. P.; Wille, C.; Nöthling, N.; Copéret, C.; Fürstner, A. Canopy Catalysts" for Alkyne Metathesis: Molybdenum Alkylidyne Complexes with a Tripodal Ligand Framework. *J. Am. Chem. Soc.* **2020**, *142*, 11279−11294. (c) Hillenbrand, J.; Leutzsch, M.; Gordon, C. P.; Copéret, C.; Fürstner, A. 183 W NMR Spectroscopy Guides the Search for Tungsten Alkylidyne Catalysts for Alkyne Metathesis. *Angew. Chem., Int. Ed.* **2020**, *59*, 21758−21768. (d) Haack, A.; Hillenbrand, J.; Leutzsch, M.; van Gastel, M.; Neese, F.; Fürstner, A. Productive Alkyne Metathesis with "Canopy Catalysts" Mandates Pseudorotation. *J. Am. Chem. Soc.* **2021**, *143*, 5643−5648.

(25) (a) Thompson, R. R.; Rotella, M. E.; Du, P.; Zhou, X.; Fronczek, F. R.; Kumar, R.; Gutierrez, O.; Lee, S. Siloxide Podand

https://doi.org/10.1021/acs.inorgchem.3c04235
Inorg. Chem. 2024, 63, 5842−5851

Ligand as a Scaffold for Molybdenum-Catalyzed Alkyne Metathesis and Isolation of a Dynamic Metallatetrahedrane Intermediate. *Organometallics* **2019**, *38*, 4054−4059. (b) Thompson, R. R.; Rotella, M. E.; Zhou, X.; Fronczek, F. R.; Gutierrez, O.; Lee, S. Impact of Ligands and Metals on the Formation of Metallacyclic Intermediates and a Nontraditional Mechanism for Group VI Alkyne Metathesis Catalysts. *J. Am. Chem. Soc.* **2021**, *143*, 9026−9039.

(26) Ge, Y.; Huang, S.; Hu, Y.; Zhang, L.; He, L.; Krajewski, S.; Ortiz, M.; Jin, Y.; Zhang, W. Highly active alkyne metathesis catalysts operating under open air condition. *Nat. Commun.* **2021**, *12*, 1136.

(27) Schrock, R. R. High Oxidation State Molybdenum and Tungsten Alkene and Alkyne Metathesis Catalysts: Where We Are and Where We Want to Go. *Adv. Synth. Catal.* **2007**, *349*, 25−25.

(28) Mayr, A.; Hoffmeister, H. Recent advances in the chemistry of metal-carbon triple bonds. *Adv. Organomet. Chem.* **1991**, *32*, 227−324.

(29) (a) Chen, S.; Liu, L.; Gao, X.; Hua, Y.; Peng, L.; Zhang, Y.; Yang, L.; Tan, Y.; He, F.; Xia, H. Addition of alkynes and osmium carbynes towards functionalized dπ-pπ conjugated systems. *Nat. Commun.* **2020**, *11*, 4651. (b) Hill, A. F.; Manzano, R. A. Dimetallapoly-yndiylidynes: Ln M≡C-(C≡C)x-C≡ML_n (x = 0−4). *Angew. Chem., Int. Ed.* **2019**, *58*, 15354−15357. (c) Frogley, B. J.; Hill, A. F. Flexible Platinum(0) Coordination to a Ditungsten Ethanediylidyne. *Angew. Chem., Int. Ed.* **2019**, *58*, 8044−8048. (d) Luo, M.; Long, L.; Zhang, H.; Yang, Y.; Hua, Y.; Liu, G.; Lin, Z.; Xia, H. Reactions of Isocyanides with Metal Carbyne Complexes: Isolation and Characterization of Metallacyclopropenimine Intermediates. *J. Am. Chem. Soc.* **2017**, *139*, 1822−1825. (e) Buil, M. L.; Cardo, J. J. F.; Esteruelas, M. A.; Oñate, E. Square-Planar Alkylidyne-Osmium and Five-Coordinate Alkylidene-Osmium Complexes: Controlling the Transformation from Hydride-Alkylidyne to Alkylidene. *J. Am. Chem. Soc.* **2016**, *138*, 9720−9728.

(30) Cui, M.; Bai, W.; Sung, H. H. Y.; Williams, I. D.; Jia, G. Robust Alkyne Metathesis Catalyzed by Air Stable d^2 Re(V) Alkylidyne Complexes. *J. Am. Chem. Soc.* **2020**, *142*, 13339−13344.

(31) Cui, M.; Sung, H. H. Y.; Williams, I. D.; Jia, G. Alkyne Metathesis with d^2 Re(V) Alkylidyne Complexes Supported by Phosphino-Phenolates: Ligand Effect on Catalytic Activity and Applications in Ring-Closing Alkyne Metathesis. *J. Am. Chem. Soc.* **2022**, *144*, 6349−6360.

(32) Cui, M.; Jia, G. Organometallic Chemistry of Transition Metal Alkylidyne Complexes Centered at Metathesis Reactions. *J. Am. Chem. Soc.* **2022**, *144*, 12546−12566.

(33) Monreal-Corona, R.; Pla-Quintana, A.; Poater, A. Predictive catalysis: a valuable step towards machine learning. *Trends Chem.* **2023**, *5*, 935.

(34) Frisch, M. J.; Trucks, G. W.; Schlegel, H. B.; Scuseria, G. E.; Robb, M. A.; Cheeseman, J. R.; Scalmani, G.; Barone, V.; Mennucci, B.; Petersson, G. A.; Nakatsuji, H.; Caricato, M.; Li, X.; Hratchian, H. P.; Izmaylov, A. F.; Bloino, J.; Zheng, G.; Sonnenberg, J. L.; Hada, M.; Ehara, M.; Toyota, K.; Fukuda, R.; Hasegawa, J.; Ishida, M.; Nakajima, T.; Honda, Y.; Kitao, O.; Nakai, H.; Vreven, T.; Montgomery, J. A., Jr.; Peralta, J. E.; Ogliaro, F.; Bearpark, M.; Heyd, J. J.; Brothers, E.; Kudin, K. N.; Staroverov, V. N.; Kobayashi, R.; Normand, J.; Raghavachari, K.; Rendell, A.; Burant, J. C.; Iyengar, S. S.; Tomasi, J.; Cossi, M.; Rega, N.; Millam, J. M.; Klene, M.; Knox, J. E.; Cross, J. B.; Bakken, V.; Adamo, C.; Jaramillo, J.; Gomperts, R.; Stratmann, R. E.; Yazyev, O.; Austin, A. J.; Cammi, R.; Pomelli, C.; Ochterski, J. W.; Martin, R. L.; Morokuma, K.; Zakrzewski, V. G.; Voth, G. A.; Salvador, P.; Dannenberg, J. J.; Dapprich, S.; Daniels, A. D.; Farkas, Ö.; Foresman, J. B.; Ortiz, J. V.; Cioslowski, J.; Fox, D. J. *Gaussian 09, Revision E.01*; Gaussian, Inc.: Wallingford, CT, 2009.

(35) (a) Becke, A. Density-functional Exchange-Energy Approximation with Correct Asymptotic Behavior. *Phys. Rev. A: At., Mol., Opt. Phys.* **1988**, *38*, 3098−3100. (b) Perdew, J. P. Density-Functional Approximation for the Correlation Energy of the Inhomogeneous Electron Gas. *Phys. Rev. B* **1986**, *33*, 8822−8824.

(36) Schäfer, A.; Huber, C.; Ahlrichs, R. Fully optimized contracted Gaussian basis sets of triple zeta valence quality for atoms Li to Kr. *J. Chem. Phys.* **1994**, *100*, 5829.

(37) (a) Küchle, W.; Dolg, M.; Stoll, H.; Preuss, H. Energy-adjusted pseudopotentials for the actinides. Parameter sets and test calculations for thorium and thorium monoxide. *J. Chem. Phys.* **1994**, *100*, 7535−7542. (b) Leininger, T.; Nicklass, A.; Stoll, H.; Dolg, M.; Schwerdtfeger, P. The accuracy of the pseudopotential approximation. II. A comparison of various core sizes for indium pseudopotentials in calculations for spectroscopic constants of InH, InF, and InCl. *J. Chem. Phys.* **1996**, *105*, 1052−1059.

(38) Zhao, Y.; Truhlar, D. G. The M06 suite of density functionals for main group thermochemistry, thermochemical kinetics, noncovalent interactions, excited states, and transition elements: two new functionals and systematic testing of four M06-class functionals and 12 other functionals. *Theor. Chem. Acc.* **2008**, *120*, 215−241.

(39) Weigend, F.; Ahlrichs, R. Balanced basis sets of split valence, triple zeta valence and quadruple zeta valence quality for H to Rn: Design and assessment of accuracy. *Phys. Chem. Chem. Phys.* **2005**, *7*, 3297−3305.

(40) Marenich, A. V.; Cramer, C. J.; Truhlar, D. G. Universal Solvation Model Based on Solute Electron Density and on a Continuum Model of the Solvent Defined by the Bulk Dielectric Constant and Atomic Surface Tensions. *J. Phys. Chem. B* **2009**, *113*, 6378−6396.

(41) (a) Atagi, L. M.; Critchlow, S. C.; Mayer, J. M. Reactivity of the tungsten carbyne W(≡CCH_3)Cl(PMe_3)$_4$: Double carbonylation, carbyne-alkyne complexes, and stoichiometric acetylene metathesis. *J. Am. Chem. Soc.* **1992**, *114*, 9223−9224. (b) Atagi, L. M.; Mayer, J. M. Reactions of the Tungsten-Carbyne Complex W(≡CMe)Cl-(PMe_3)$_4$ with π-Acceptor Ligands: Carbon Monoxide, Alkynes, and Alkenes. *Organometallics* **1994**, *13*, 4794−4803.

(42) (a) Zhu, C.; Yang, Y.; Luo, M.; Yang, C.; Wu, J.; Chen, L.; Liu, G.; Wen, T.; Zhu, J.; Xia, H. Stabilizing Two Classical Antiaromatic Frameworks: Demonstration of Photoacoustic Imaging and the Photothermal Effect in Metallaaromatics. *Angew. Chem., Int. Ed.* **2015**, *54*, 6181−6185. (d) Das, U. Closed-shell and Open-Shell Ferracyclobutadienes-Syntheses, Characterization and Reactivity Studies. Dissertation Thesis, University of Bonn (Mensch & Buch: Berlin, 2014.

(43) (a) Mayer, I. Charge, bond order and valence in the AB initio SCF theory. *Chem. Phys. Lett.* **1983**, *97*, 270−274. (b) Mayer, I. Bond order and valence: Relations to Mulliken's population analysis. *Int. J. Quantum Chem.* **1984**, *26*, 151−154.

(44) Examples of MBO applications: (a) Poater, J.; Gimferrer, M.; Poater, A. Covalent and Ionic Capacity of MOFs To Sorb Small Gas Molecules. *Inorg. Chem.* **2018**, *57*, 6981−6990. (b) Poater, A.; Vummaleti, S. V. C.; Pump, E.; Cavallo, L. Comparing Ru and Fe-catalyzed olefin metathesis. *Dalton Trans.* **2014**, *43*, 11216−11220. (c) Poater, A.; Cavallo, L. Mechanistic Insights into the Double C-H (De)Activation Route of a Ru-based Olefin Metathesis Catalyst. *J. Mol. Catal. A Chem.* **2010**, *324*, 75−79.

(45) Examples of MBOs lower than the expected: (a) Ahmadi, M.; Panahi, F.; Bahri-Laleh, N.; Sabzi, M.; Pareras, G.; Falcone, B. N.; Poater, A. pH-Responsive Gelation in Metallo-Supramolecular Polymers Based on the Protic Pyridinedicarboxamide Ligand. *Chem. Mater.* **2022**, *13*, 6155−6169. (b) Tabrizi, M.; Sadjadi, S.; Pareras, G.; Nekoomanesh-Haghighi, M.; Bahri-Laleh, N.; Poater, A. Efficient hydro-finishing of polyalfaolefin based lubricants under mild reaction condition using Pd on ligands decorated halloysite. *J. Colloid Interface Sci.* **2021**, *581*, 939−953. (c) Hanifpour, A.; Bahri-Laleh, N.; Nekoomanesh-Haghighi, M.; Poater, A. 1-Decene Oligomerization by New Complexes Bearing Diamine-Diphenolates Ligands: Effect of Ligand Structure. *Appl. Organomet. Chem.* **2021**, *35*, No. e6227. (d) Poater, A.; Ragone, F.; Correa, A.; Cavallo, L. Comparison of different ruthenium−alkylidene bonds in the activation step with N-heterocyclic carbene Ru-catalysts for olefins metathesis. *Dalton Trans.* **2011**, *40*, 11066−11069. (e) Poater, A.; Moradell, S.; Pinilla, E.; Poater, J.; Solà, M.; Martínez, M. A.; Llobet, A. A trinuclear Pt(II)

https://doi.org/10.1021/acs.inorgchem.3c04235
Inorg. Chem. 2024, 63, 5842−5851

compound with short Pt−Pt−Pt contacts. An analysis of the influence of $\pi-\pi$ stacking interactions on the strength and length of the Pt−Pt bond. *Dalton Trans.* **2006**, 1188−1196. (f) Poater, A.; Ragone, F.; Correa, A.; Cavallo, L. Exploring the Reactivity of Ru-Based Metathesis Catalysts with a π-Acid Ligand Trans to the Ru-ylidene Bond. *J. Am. Chem. Soc.* **2009**, *131*, 9000−9006.

(46) (a) Rây, P.; Dutt, N. K. Kinetics and mechanism of racemisation of optically active cobaltic tris biguanide complex. *J. Indian Chem. Soc.* **1943**, *20*, 8192. (b) Rodger, A.; Johnson, B. F. G. Which Is More Likely: The Ray-Dutt Twist or the Bailar Twist? *Inorg. Chem.* **1988**, *27*, 3061−3062. (c) Ghosh, R. Priyadaranjan Rây: Contributions to Chemical Science. *Resonance* **2021**, *26*, 73−87.

(47) Kozuch, S.; Shaik, S. How to Conceptualize Catalytic Cycles? The Energetic Span Model. *Acc. Chem. Res.* **2011**, *44*, 101−110.

(48) (a) Davis, A. V.; Firman, T. K.; Hay, B. P.; Raymond, K. N. d-Orbital Effects on Stereochemical Non-Rigidity: Twisted Ti^{IV} Intramolecular Dynamics. *J. Am. Chem. Soc.* **2006**, *128*, 9484−9496. (b) Rzepa, H. S.; Cass, M. E. In Search of the Bailar and Rây−Dutt Twist Mechanisms That Racemize Chiral Trischelates: A Computational Study of Sc^{III}, Ti^{IV}, Co^{III}, Zn^{II}, Ga^{III}, and Ge^{IV} Complexes of a Ligand Analogue of Acetylacetonate. *Inorg. Chem.* **2007**, *46*, 8024−8031.

(49) (a) Maloney, M. P.; Stenfors, B. A.; Helquist, P.; Norrby, P.-O.; Wiest, O. Interplay of Computation and Experiment in Enantioselective Catalysis: Rationalization, Prediction, and—Correction? *ACS Catal.* **2023**, *13*, 14285−14299. (b) Monreal-Corona, R.; Díaz-Jiménez, À.; Roglans, A.; Poater, A.; Pla-Quintana, A. Indolizine Synthesis through Annulation of Pyridinium 1,4-Thiolates and Copper Carbenes: A Predictive Catalysis Approach. *Adv. Synth. Catal.* **2023**, *365*, 760−766. (c) Escayola, S.; Bahri-Laleh, N.; Poater, A. $\%V_{Bur}$ index and steric maps: from predictive catalysis to machine learning. *Chem. Soc. Rev.* **2024**, *53*, 853−882.

(50) (a) Poater, A.; Cosenza, B.; Correa, A.; Giudice, S.; Ragone, F.; Scarano, V.; Cavallo, L. SambVca: A Web Application for the Calculation of the Buried Volume of N-Heterocyclic Carbene Ligands. *Eur. J. Inorg. Chem.* **2009**, *2009*, 1759−1766. (b) Falivene, L.; Credendino, R.; Poater, A.; Petta, A.; Serra, L.; Oliva, R.; Scarano, V.; Cavallo, L. SambVca 2. A Web Tool for Analyzing Catalytic Pockets with Topographic Steric Maps. *Organometallics* **2016**, *35*, 2286−2293. (c) Falivene, L.; Cao, Z.; Petta, A.; Serra, L.; Poater, A.; Oliva, R.; Scarano, V.; Cavallo, L. Towards the online computer-aided design of catalytic pockets. *Nat. Chem.* **2019**, *11*, 872−879.

https://doi.org/10.1021/acs.inorgchem.3c04235
Inorg. Chem. 2024, 63, 5842−5851